



EVOLUTIONARY METHODS FOR THE APPROXIMATION OF THE STABILITY DOMAIN AND FREQUENCY OPTIMIZATION OF CONSERVATIVE MAPS

Y. G. PETALAS*, C. G. ANTONOPOULOS[†], T. C. BOUNTIS[†]
and M. N. VRAHATIS*

**Computational Intelligence Laboratory (CI Lab),
Department of Mathematics, University of Patras,
GR-26110 Patras, Greece*

*University of Patras Artificial Intelligence Research Center (UPAIRC),
University of Patras, GR-26110 Patras, Greece*

*[†]Center for Research and Applications of Nonlinear Systems (CRANS),
Department of Mathematics, University of Patras,
GR-26110 Patras, Greece*

Received August 9, 2007; Revised November 27, 2007

Two methodologies are presented for the numerical approximation of the “domain of stability” of nonlinear conservative maps: (a) the Evolutionary Estimation of the Domain of Stability (EEDS) and (b) the Evolutionary Frequency Optimization (EFO), optimizing certain frequency parameters of these maps so that the domain of stability encompasses the maximum possible “volume” of bounded motion, known in the accelerator literature as the dynamic aperture. The central components of the proposed approaches are: The Differential Evolution algorithm (DE) based on concepts of Computational Intelligence and the method of the Smaller ALignment Index (SALI) used for the determination of chaotic dynamics. Initially, we give a brief description of the two methodologies and then demonstrate their usefulness by applying them to some well-known examples of 2D and 4D Hénon maps. The proposed methodologies can be easily applied to “volume” preserving maps which are not necessarily symplectic as well as to continuous dynamical systems (flows) and can also be generalized to treat conservative dynamical systems of any dimension.

Keywords: Conservative maps; domain of stability; chaotic regions; the SALI method; evolutionary methods; accelerator maps.

1. Introduction

Conservative maps and in particular symplectic ones, represent discrete versions of Hamiltonian systems which arise in many applications including particle accelerators, plasma physics and fluid dynamics [Meiss, 1992]. An important example in this class are symplectic mappings used to model betatron motion in the storage ring of high energy accelerators [Scandale & Turchetti, 1991; Todesco &

Giovannozzi, 1996; Vrahatis *et al.*, 1997]. If the particles are protons (or antiprotons) radiation effects can be neglected and a turn around such as a ring can be described by a symplectic map. This map has a unique fixed point corresponding to the ideal circular orbit of particles passing through the center of the ring. Storage rings are constructed in such a way as to make the fixed point elliptic, so that particles with initial conditions within a small neighborhood

of the fixed point remain inside that neighborhood under the repeated action of the symplectic map in the linear approximation.

In this paper, we study Hénon type symplectic maps of two (2D) and four (4D) dimensions which describe the effects of a particle's motion through nonlinear magnetic focusing elements of the FODO cell type [Scandale & Turchetti, 1991; Todesco & Giovannozzi, 1996; Vrahatis *et al.*, 1997; Vrahatis, 1995; Bazzani *et al.*, 1994].

The 2D Hénon map is given by the set of equations

$$\begin{aligned}x' &= \cos(2\pi v_x)x + \sin(2\pi v_x)(p_x + x^2), \\p'_x &= -\sin(2\pi v_x)x + \cos(2\pi v_x)(p_x + x^2),\end{aligned}$$

and the 4D Hénon map is given by

$$\begin{aligned}x' &= \cos(2\pi v_x)x + \sin(2\pi v_x)(p_x + (x^2 - y^2)), \\p'_x &= -\sin(2\pi v_x)x + \cos(2\pi v_x)(p_x + (x^2 - y^2)), \\y' &= \cos(2\pi v_y)y + \sin(2\pi v_y)(p_y - 2xy), \\p'_y &= -\sin(2\pi v_y)y + \cos(2\pi v_y)(p_y - 2xy).\end{aligned}$$

The x, y variables are the deviations of the particle's motion from the ideal circular trajectory in the horizontal and vertical directions, respectively and p_x, p_y are the corresponding momenta. Variables v_x, v_y are the linear tunes of the accelerator machine.

As is well known, the nonlinearities that appear in the above equations can deflect particles far from the fixed point under repeated application of the map, causing them eventually to be removed from the beam. Thus, it is of crucial importance for the efficient operation of the accelerator and successful outcome of the experiments to identify the largest possible region in phase space, where one can safely avoid severe particle loss and decrease of the beam's luminosity [Scandale & Turchetti, 1991; Todesco & Giovannozzi, 1996; Vrahatis *et al.*, 1997; Vrahatis, 1995; Bazzani *et al.*, 1994]. An accurate estimate of this domain yields the so-called *dynamic aperture*, as it is called in the accelerator literature.

In the 2D case, it is well known that there exists a *last* KAM torus that divides the two-dimensional phase space into two disjoint domains in the following sense: It is a continuous, but in general non-differentiable curve, beyond which no closed curves exist surrounding the origin [Todesco & Giovannozzi, 1996; Bazzani *et al.*, 1994; MacKay & Meiss, 1987]. As we cannot locate this particular curve,

with our method, we call “boundary of stability” the closest possible smooth approximation of this curve bounding a region around the origin called G . Orbits corresponding to initial conditions in the interior of G remain inside G for an infinite number of iterations of the map.

Of course, within G there also exist initial conditions corresponding to unstable periodic orbits. These orbits possess small regions of chaotic motion around them, which also remain forever within G . In the case of 2D maps, orbits starting within G never pass outside the boundary of stability since this consists of a closed curve which separates the two-dimensional plane into disjoint regions. On the other hand, outside this boundary there exist chains of islands, as well as initial conditions corresponding to chaotic orbits that escape to infinity after a small number of iterations.

In the 4D case, the tori are two-dimensional and do not divide the four-dimensional phase space into disjoint regions. Chaotic layers are no longer separated by invariant surfaces and can be connected, allowing orbits to move away from the origin and finally escape to infinity. However, we have found that there is a large part of phase space around the origin, in which initial conditions are stable for a very long time. In this region there are instabilities related to the so-called Arnold diffusion [Chirikov, 1979] but they are so slow that the corresponding orbits can be practically considered stable. Outside this region, chaos is dominant and the majority of the initial conditions escape to infinity after a finite time. Furthermore, in such 4D maps the meaning of phase space “volume” in which orbits remain bounded for a very long time is not at all clear, since the corresponding domain of stability cannot be defined as precisely as in the 2D case.

In this paper, we propose two methodologies: The first one is named Evolutionary Estimation of the Domain of Stability (EEDS) and its primary aim is to estimate approximately the “domain of stability” of conservative maps which contains the maximum possible “volume” of bounded orbits. The second is called Evolutionary Frequency Optimization (EFO), treating the frequency(ies) of a map as parameters of a maximization problem. The aim of this optimization is to find parameter values ensuring the maximum such possible “volume” of bounded motion for the dynamics of the map. EEDS will be a component in the solution of this maximization problem.

Both methodologies combine the following well-known techniques of nonlinear dynamics theory and computational intelligence [Engelbrecht, 2002]:

- (a) The correlation dimension [Grassberger & Procaccia, 1983a, 1983b] for the estimation of the dimension of particular set points that are produced by the proposed methodologies.
- (b) The Differential Evolution (DE) [Storn & Price, 1997; Corne *et al.*, 1999] algorithm for the optimization issues that arise in the proposed methodologies.
- (c) The Smaller ALignment Index (SALI) [Skokos, 2001] which is used for the efficient and fast detection of chaotic motion in conservative dynamical systems (flows and/or maps).

Our paper is organized as follows: In Sec. 2, we give the necessary background material, by describing the SALI method and the DE algorithm. The two proposed evolutionary methodologies are presented in Sec. 3. Furthermore, the experimental results obtained from the application of EEDS and EFO to the Hénon symplectic maps in 2 and 4 dimensions are detailed in Sec. 4. The paper ends with concluding remarks in Sec. 5.

2. Background Material

2.1. Smaller ALignment Index (SALI)

The SALI method was initially introduced in [Skokos, 2001] and has already been successfully applied to distinguish ordered from chaotic orbits in maps of various dimensions [Bountis & Skokos, 2006a, 2006b], in Hamiltonian systems [Skokos *et al.*, 2003a, 2003b, 2004], as well as in problems of Celestial Mechanics [Széll, 2003, 2004], Galactic Dynamics [Manos & Athanassoula, 2005a, 2005b], Field Theory [De Assis *et al.*, 2005] and nonlinear one-dimensional lattices [Antonopoulos *et al.*, 2006; Antonopoulos & Bountis, 2006a; Panagopoulos *et al.*, 2004].

Let us consider the M -dimensional phase space of an arbitrary conservative dynamical system, for example a symplectic map of even dimension $M = 2m$, $m \in \mathbb{N}$. In this case, an initial condition $X^0 = (x_1^0, x_2^0, \dots, x_M^0)$ of the map evolves according to the equations of motion

$$X^{n+1} = \Phi(X^n), \quad (1)$$

where n is the number of iterations and $X^n = (x_1^n, x_2^n, \dots, x_M^n)$ denotes the n th iteration of the map.

In order to determine the chaotic or ordered nature of a particular orbit of the map (1) with initial condition X^0 , we follow the evolution of two initially linearly independent deviation vectors V_1^0 and V_2^0 . Their evolution in time is governed by the so-called *tangent map* equations

$$V_i^{n+1} = D\Phi(X^n) \cdot V_i^n, \quad i = 1, 2 \quad (2)$$

where $V_i^n = (dv_{i,1}^n, dv_{i,2}^n, \dots, dv_{i,M}^n)$ and $D\Phi(X^n)$ is the Jacobian matrix of the equations of motion (1).

The evaluation of the SALI is then accomplished by computing the quantity

$$\text{SALI}(n) = \min \left\{ \left\| \frac{V_1^n}{\|V_1^n\|} + \frac{V_2^n}{\|V_2^n\|} \right\|, \left\| \frac{V_1^n}{\|V_1^n\|} - \frac{V_2^n}{\|V_2^n\|} \right\| \right\}, \quad (3)$$

where $\|\cdot\|$ denotes the usual Euclidean distance of the argument.

According to the above definition, two distinct cases exist in general:

- (a) The orbit under consideration is *chaotic*. Then the two deviation vectors tend to become aligned in the most unstable nearby direction corresponding to the maximal Lyapunov exponent of the orbit under consideration. Thus, the SALI tends to *zero* exponentially with a slope that depends on the two largest Lyapunov exponents [Skokos *et al.*, 2003].
- (b) The orbit under consideration is *regular* or *quasiperiodic*, hence there is no preferred direction in which the vectors can become aligned since the Lyapunov exponents are all zero. The two deviation vectors tend to become tangent to the torus on which the orbit is evolving and, in general, have different directions, making the SALI fluctuate around *nonzero* positive values [Skokos *et al.*, 2004]. An exception exists in the case of 2D maps, where SALI tends to zero following a power law of the form $\propto n^{-1}$ (see [Skokos, 2001] for more details).

It is thus clear that SALI behaves differently in the cases of ordered and chaotic orbits and this makes it a powerful, simple and easy criterion to implement numerically. It is well suited for multidimensional systems and is especially rapid and reliable for $2N$ -dimensional symplectic maps.

2.2. Differential evolution

Differential Evolution (DE) [Storn & Price, 1997] is a population-based algorithm for the global optimization of multimodal N -dimensional functions. It attains a set of possible solutions for the problem under consideration and evolves them in order to find the “best” one. The meaning of the term “best” will become clear below when we present the distinct steps one follows for the application of the DE algorithm. Some of the advantages of the DE algorithm are the following:

- (a) It can operate on nondifferentiable and/or discontinuous functions of arbitrary dimensions.
- (b) It can be applied in functions contaminated by noise or functions that change dynamically over time.
- (c) It can be applied to integer, discrete and mixed programming problems.
- (d) Finally, it can be easily computer-parallelized [Plagianakos & Vrahatis, 2002].

More specifically, the DE algorithm is said to exploit a population of individuals (N -dimensional vectors). Let u_g^i denote the i th individual of the population in the g th iteration of the algorithm. Then, DE is described by the following four distinct steps:

Step 1 (Initialization step). Initialize randomly the individuals of the population. Set the mutation factor, F , and the recombination (cross-over) factor, CR , to fixed values within the interval $[0, 1]$ and choose an *objective function* for the problem under study.

Step 2 (Mutation step). Mutate each individual u_g^i (called the target individual) of the population to form a trial vector, v_{g+1}^i , by applying one of the following operators,

$$v_{g+1}^i = u_g^{r1} + F(u_g^{r2} - u_g^{r3}), \quad \text{DE1}$$

$$v_{g+1}^i = u_g^{r1} + F(u_g^{r2} - u_g^{r3}) + F(u_g^{r4} - u_g^{r5}), \quad \text{DE2}$$

$$v_{g+1}^i = u_g^{\text{best}} + F(u_g^{r1} - u_g^{r2}), \quad \text{DE3}$$

$$v_{g+1}^i = u_g^i + F(u_g^i - u_g^{\text{best}}) + F(u_g^{r1} - u_g^{r2}), \quad \text{DE4}$$

$$v_{g+1}^i = u_g^{\text{best}} + F(u_g^{r1} - u_g^{r2}) + F(u_g^{r3} - u_g^{r4}), \quad \text{DE5}$$

where $r1, r2, r3, r4$ are random integers such that, $r1 \neq r2 \neq r3 \neq r4 \neq i \neq \text{best}$. The index *best* is used to represent the individual with the best objective function value in the current population. Throughout the paper, the **DE2** operator was used.

Step 3 (Recombination (Crossover) step). For each element of the trial vector, v_{g+1}^i , obtain a random value, $r \in [0, 1]$. If $r \leq CR$, set $u_{g+1}^i = v_{g+1}^i$, otherwise set $u_{g+1}^i = u_g^i$.

Step 4 (Selection step). For each individual of the population u_{g+1}^i evaluate its value through the objective function. If this value is better than the one of the target individual u_g^i , then the individual u_{g+1}^i replaces the target individual in the next iteration. Otherwise, the target individual is retained in the next iteration of the DE algorithm. If the termination criterion is not satisfied, then go to the second step. As a termination criterion we can use a predefined number of iterations or an error goal value of the objective function.

3. The Proposed Methodologies

3.1. Evolutionary estimation of the domain of stability (EEDS) of conservative maps

The aim of the EEDS is to approximate numerically the “domain of stability” surrounding the maximum possible “volume” of bounded orbits in the phase space. To do this, we locate first a point, as close as possible to the boundary of this domain, which we call from now on, the *last point*. The consecutive iterations of the map having this point as initial condition will produce a set of points which we shall call the “object”. This “object” is considered as a candidate for the determination of the “domain” of stability of the above map, in the sense that at closer distances from the origin no orbit is observed to escape, up to 10^8 iterations.

EEDS first solves an optimization problem in order to find the minimum/maximum distance between the central elliptic point and the “object”. Using the output of the optimization problem, EEDS finds the last point and afterwards the associated “object”. The main components of EEDS are the DE algorithm, the SALI method and the correlation dimension. The individuals of the DE algorithm are points in the phase space of the map that serve as initial conditions for the SALI method. When SALI encounters the first chaotic orbit (that is, SALI becomes less than a given very small threshold), its corresponding initial condition is a *possible candidate* point belonging to the “object”. Next, for the

sake of improving our prediction, we further iterate the map (using as initial condition this particular point) for thousands of iterations to see whether the orbit escapes to infinity. If it does not, then we assume that it is sufficiently close to the “object”.

Additionally, in order to achieve an even better precision, we use the one-dimensional bisection method [Vrahatis, 1995] combined with the SALI algorithm. The two end-points of the bisection method are the origin of the map and the last point found by the above procedure. Here, the SALI method plays the role of the objective function, used in the bisection method. The output point resulting from the application of the bisection method is used as an approximate closest point “lying” on the “object”.

Consequently, we calculate the Euclidean distance between the last point and the origin of the map. This distance will be the value of the objective function for the particular individual. If we are looking for the maximum and/or minimum distance between the origin and the “object”, the *best* direction will be the one with the maximum or minimum distance proposed by the application of the above DE algorithm. We then repeat the steps of the DE algorithm to evolve the population for more iterations in order to obtain as good estimates as possible.

After the termination of the DE algorithm, in order to obtain even better accuracy we use as radial directions the optimum individual and the individuals with objective function values worse than the optimum value within 5%. Then, we move, in every such direction, with small steps 0.003 from the origin and iterate the map for 100,000 iterations. Thus, for each individual, we record the last point for which the orbit remains bounded under these iterations and calculate the Euclidean distance between this last point and the origin of the map. This distance is the new objective function value. After this, we use the final optimum individual and its corresponding objective function to calculate the last point in phase space for which bounded motion is ensured. The iterations of the map with this point as an initial condition will fully produce the desired “object” mentioned above. Finally, the calculation of the correlation dimension [Grassberger & Procaccia, 1983a, 1983b] of the “object” will be a satisfactory indication of the closeness of this point to the domain of stability of the map.

Below, we highlight the key-points of EEDS:

- (1) The individuals u_g^i of the DE are directions (initially random) in the phase space.
- (2) The objective function output is the distance between the origin (elliptic fixed point) and the last point found in each direction.
- (3) The last point is an approximated point for the “object”.
- (4) The last point is found by using the SALI and the bisection method.
- (5) The directions are evolved using the DE operators.
- (6) Output of the optimization scheme is the minimum/maximum distance (direction) between the origin and the “object”. (Also, available are statistics on intermediate distances.)
- (7) Using the last point associated with the minimum/maximum distance as initial condition, we follow it for a given number of iterations to verify that the orbit does not escape to infinity.
- (8) This set of points (“object”) is assumed to be an approximation of the domain of stability of the map.
- (9) The estimation of the dimension of this set of points is accomplished by using the correlation dimension.

3.2. *Evolutionary frequency optimization (EFO) of conservative maps*

The frequencies appearing in the two maps considered in this paper are constant parameters that can be changed by the experimentalist, whose values are crucial for the success of the experiment. They may lead to beam diffusion or safe operation, keeping the largest possible number of particles bounded for the greatest number of turns inside the storage rings of the accelerator.

Here, we propose a way to treat these frequencies as parameters in an optimization problem, whose objective function has as output the largest possible region of stability around the origin of the map. Thus, it is a maximization problem. The determination of the objective function for this problem makes use of the EEDS method already introduced in Sec. 3.1 to study the region and last domain of stability of the Hénon 2D and 4D symplectic maps with specific constant frequencies.

Thus, we use once more the DE algorithm to solve the new optimization problem. This time, the individuals are sets of frequency(ies) of the

map. So, the DE algorithm has a population of frequency(ies) which evolves according to the prescribed DE steps of Sec. 2.2. The objective function, we propose, is a weighted sum of three factors and will be computed by EEDS for every individual (frequency(ies)). These factors are

- (a) The correlation dimension of the resulting “object”.
- (b) The mean value of the distances of the points of the “object” from the central elliptic point of the map.
- (c) The perturbation of some randomly chosen points of this “object”. Each chosen point is slightly perturbed and new points are produced in the phase space.

The perturbation procedure consists of two parts: First, we produce points with directions towards the elliptic point (“inner” points), while in the second part points are produced in the opposite direction (“outer” points). Each produced point will serve as an initial condition of the map for a given number of iterations. The number of iterations for which the orbit stays bounded are recorded and their mean values are computed for the “inner” and “outer” perturbed points. Finally, the third factor is the difference between these values (mean “inner” – mean “outer”) divided by the maximum number of iterations of the map.

4. Results

4.1. Application of EEDS to the 2D Hénon map

In the 2D Hénon case, EEDS was applied for a variety of constant tunes ν_x lying in the interval $[0.1, 0.45]$ with tune step 0.025. For every tune ν_x , ten different experiments were performed. The population of the DE algorithm was set to 10 and the mutation and crossover factors F , CR equal to 0.5. The chaoticity threshold for the SALI method was set to 10^{-8} as in references [Skokos, 2001; Skokos *et al.*, 2003a, 2003b], while for the bisection method it was set to 10^{-6} . The number of iterations of the map used in the SALI computation was 500. When the SALI was used in combination with the bisection method, the number of iterations was decreased to 100.

In every single experiment, the goal of the DE algorithm was to find the minimum distance between the central elliptic point (origin of the 2D

map) and the “object”. We followed this approach because we noticed that the boundary of stability was approximated more accurately by iterations starting with the point associated with the *minimum* distance found by the DE algorithm. After locating this point, the map was iterated an additional 10^5 times, producing at the end an “object”. For every such produced “object”, the maximum and minimum distances from the origin were also computed. In Fig. 1, we have displayed for the 2D Hénon map with the frequency $\nu_x = 0.45$, the last invariant curve (red curve), the minimum (blue line) and maximum distance (green line) of this curve from the central elliptic point.

To test the validity of our approach on the 2D Hénon map, we also calculated an approximation of the last invariant curve by *ad hoc* methods, following a particular radial direction outward and applying the map equations until an orbit escaped in less than 10^8 iterations. These approximate values are then compared with the corresponding ones obtained by EEDS for a wide range of frequencies in Figs. 2(a) and 2(b). In particular, in Fig. 2(a) the results concerning the maximum distance are shown, while in Fig. 2(b) we exhibit those of the minimum distance. As the two plots in these figures

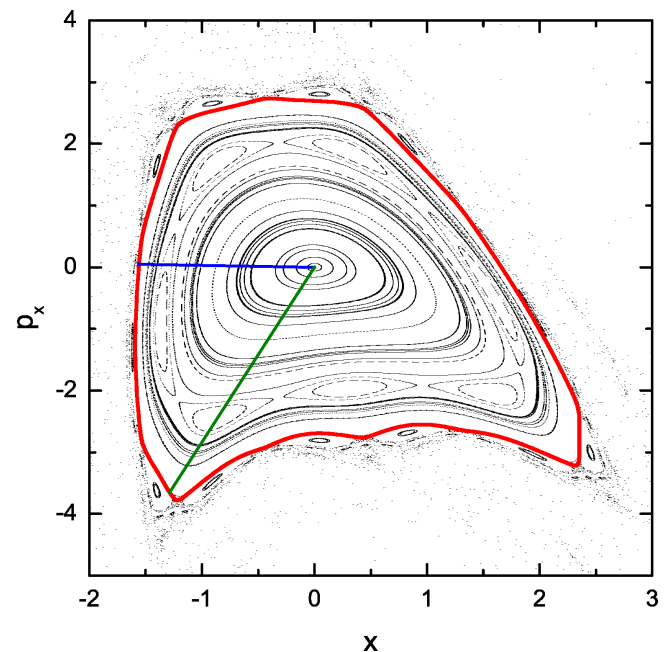


Fig. 1. Phase portrait of the 2D Hénon map for the frequency $\nu_x = 0.45$, showing the approximate last invariant curve (red curve) by indicating via a blue line its minimum distance from the origin and by a green line its maximum distance from the origin.

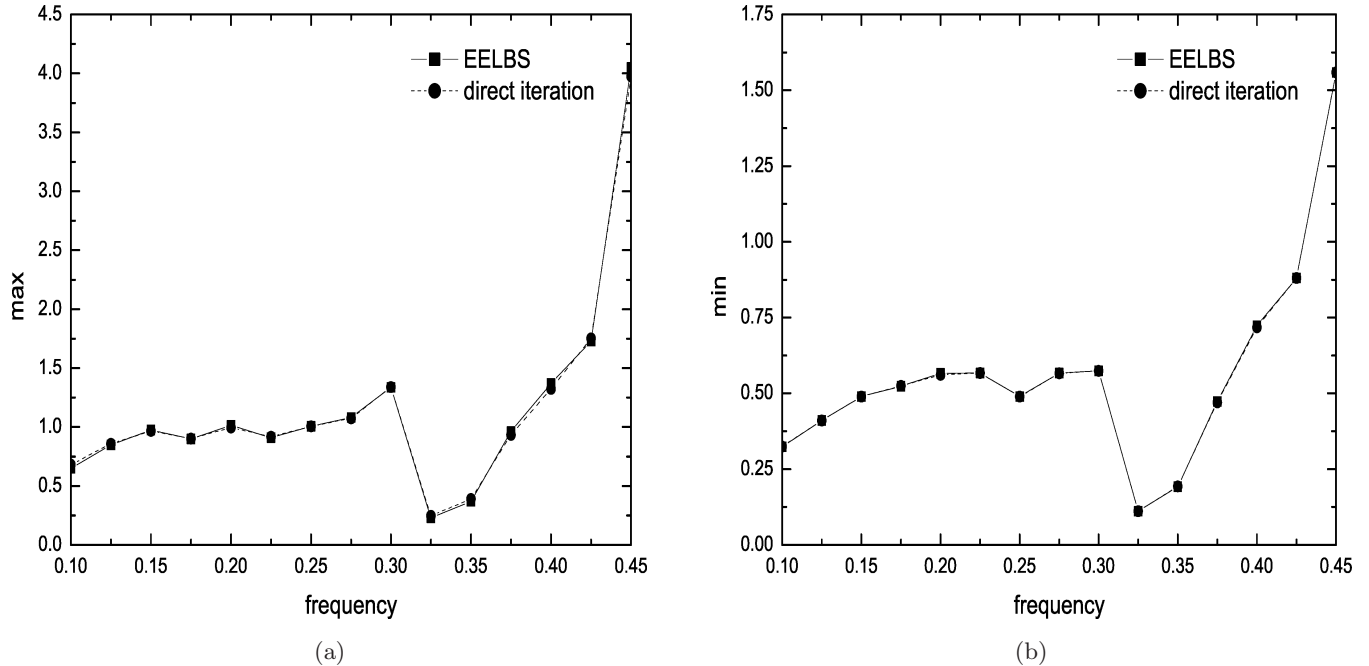


Fig. 2. (a) Plots of the maximum distance (from the origin) of the points produced by EEDS together with points of the corresponding objects obtained by direct iteration of the 2D Hénon map. Note that at this level of resolution the two plots are indistinguishable. (b) Similarly for the points at minimum distance from the origin.

are practically identical, we conclude that our evolutionary approach achieves indeed very accurate predictions for the last invariant curve, compared to what is found by inspection of the phase space of the map.

4.2. Application of EEDS to the 4D Hénon map

We now turn to the 4D Hénon map. Here, EEDS was applied using as starting point the tunes $v_x = 0.61903$ and $v_y = 0.4152$, which we had found in an earlier publication [Vrahatis *et al.*, 1997]. The remaining parameters of EEDS (DE, SALI, bisection settings) are the same as in the 2D case. The population was set to be 20 and the number of iterations of the 4D map used in the SALI method was 1000. Thirty experiments in total were performed. Again, as in the 2D case, the goal of the DE algorithm is to find the minimum distance between the elliptic point (or origin of the map) and the “object” of the 4D Hénon map, in the sense explained in the earliest sections.

After the estimation of the last point, the map was iterated for 5×10^5 iterations with this point as initial condition. For the produced “object”, we also computed its maximum, minimum and mean

distances from the central elliptic point, as well as its correlation dimension. In 20 out of a total of 30 experiments, the resulting “object” was an orbit that remained bounded for 5×10^5 iterations without escaping to infinity. Due to the stochastic nature of the algorithm, and the complexity of phase space, in each experiment we notice that a different geometric “object” is produced.

In Table 1, statistical results are presented concerning the minimum, maximum and mean distances calculated in the above mentioned 20 experiments. Note that the minimum distances are especially characterized by the smallest standard deviation. This observation agrees well with a similar one made earlier in the 2D case and leads to the conclusion that it is preferable to estimate the minimum distance of the “object” with respect to the central point, in every case.

Table 1. Statistics for the distances of the points of the “object” of the 4D Hénon map from the central elliptic point.

Values	Max	Min	Mean	St. Dev.
Minimum distance	0.54	0.50	0.52	0.01
Maximum distance	1.13	0.92	1.04	0.06
Mean distance	0.82	0.67	0.74	0.05

Table 2. The associated last points (first–fourth column), Correlation Dimension (C.D.) with 5×10^{-3} accuracy (fifth column) and Mean Distances (M.D.) from the central elliptic point (sixth column) of the 20 experiments that did not escape up to 5×10^5 iterations for the 4D Hénon map produced by EEDS for the pair of tunes $\nu_x = 0.61903$ and $\nu_y = 0.4152$. The columns of the table are sorted in increasing order of magnitude of the Mean Distances.

x	p_x	y	p_y	C.D.	M.D.
−0.609705	0.130127	−0.010712	0.002023	0.94	0.8199
−0.598295	0.143924	0.035110	−0.014355	0.90	0.8139
−0.626369	0.108863	−0.035885	0.024461	0.89	0.8138
−0.596637	0.142641	−0.012402	0.026018	0.92	0.8100
0.395261	0.246253	−0.265755	−0.364423	2.89	0.7423
0.382272	0.193950	−0.197602	−0.470238	2.93	0.7407
0.387442	0.229748	−0.234129	−0.412568	2.81	0.7393
0.376212	0.276229	−0.264512	−0.381121	2.92	0.7349
0.400782	0.195349	−0.274080	−0.406305	2.74	0.7292
0.387985	0.275856	−0.294545	−0.341922	2.18	0.7217
0.384996	0.308129	−0.285890	−0.297610	2.18	0.7214
0.382419	0.282068	−0.270252	−0.328869	2.19	0.7204
0.376927	0.260405	−0.274911	−0.381446	2.74	0.7193
0.364460	0.262546	0.257946	0.418398	2.23	0.7163
0.402795	0.231527	−0.243043	−0.337608	2.05	0.7146
0.397762	0.231556	−0.186804	−0.343580	2.06	0.6965
0.385228	0.292131	0.237883	0.321652	2.03	0.6890
0.387955	0.241097	−0.191632	−0.366308	2.06	0.6772
0.397729	0.260177	−0.223117	−0.317848	2.36	0.6719
0.404900	0.114807	−0.122447	−0.457707	2.13	0.6684

In Table 2, we exhibit results concerning the initial conditions of the last points (first–fourth column), correlation dimension with 5×10^{-3} accuracy (fifth column) and mean distances from the central elliptic point (sixth column) for all orbits that did not lead to escape up to 5×10^5 iterations for the 4D Hénon map for $\nu_x = 0.61903$ and $\nu_y = 0.4152$. The columns of the table are sorted in increasing order of magnitude of the mean distances. Thus, we can identify three groups of objects with respect to their correlation dimension: There are four objects with correlation dimension around 1, ten objects with correlation dimension around 2 and the remaining six objects have correlation dimension greater than 2.7.

4.2.1. A study of three examples

Let us now study one example from each of the above three categories, which for convenience we shall call objects 1–3. Object 1 corresponds to the first line of Table 2, object 2 to the 17th line and object 3 to the 13th line of the same table. In Figs. 3(a)–3(c), the three-dimensional projection x, p_x, y of the 4D map and its two-dimensional

projections are exhibited respectively for objects 1–3.

The correlation dimension of each object was calculated using the TISEAN package of time series analysis [Hegger *et al.*, 1999]. In Figs. 4(a)–4(c), the plot $\log_2 C_2^d(r) / \log_2 r$ versus $\log_2 r$ is presented while in Figs. 5(a)–5(c) $\log_2 C_2^d(r)$ versus $\log_2 r$, where $C_2^d(r)$ is the correlation integral and $r \rightarrow 0$. The first 10^5 points of the object were used with embedding dimension $m = 8$ and delay $\tau = 1$, while the Theiler window was set to be 60 as in [Vrahatis *et al.*, 1997].

In Figs. 4(a)–4(c) the correlation dimension is estimated from a horizontal straight line corresponding to the so-called “plateau” of the figure. This plateau is located by searching for an interval that is horizontal with the minimum possible standard deviation whose mean value is the output of the estimated correlation dimension. In Figs. 5(a)–5(c), the same correlation dimension is also estimated by the slope of the diagram. This slope was numerically approximated by the method of linear fitting corresponding to embedding dimensions $m \geq 4$. Thus, from both figures we deduce that the correlation dimension for object 1 is about

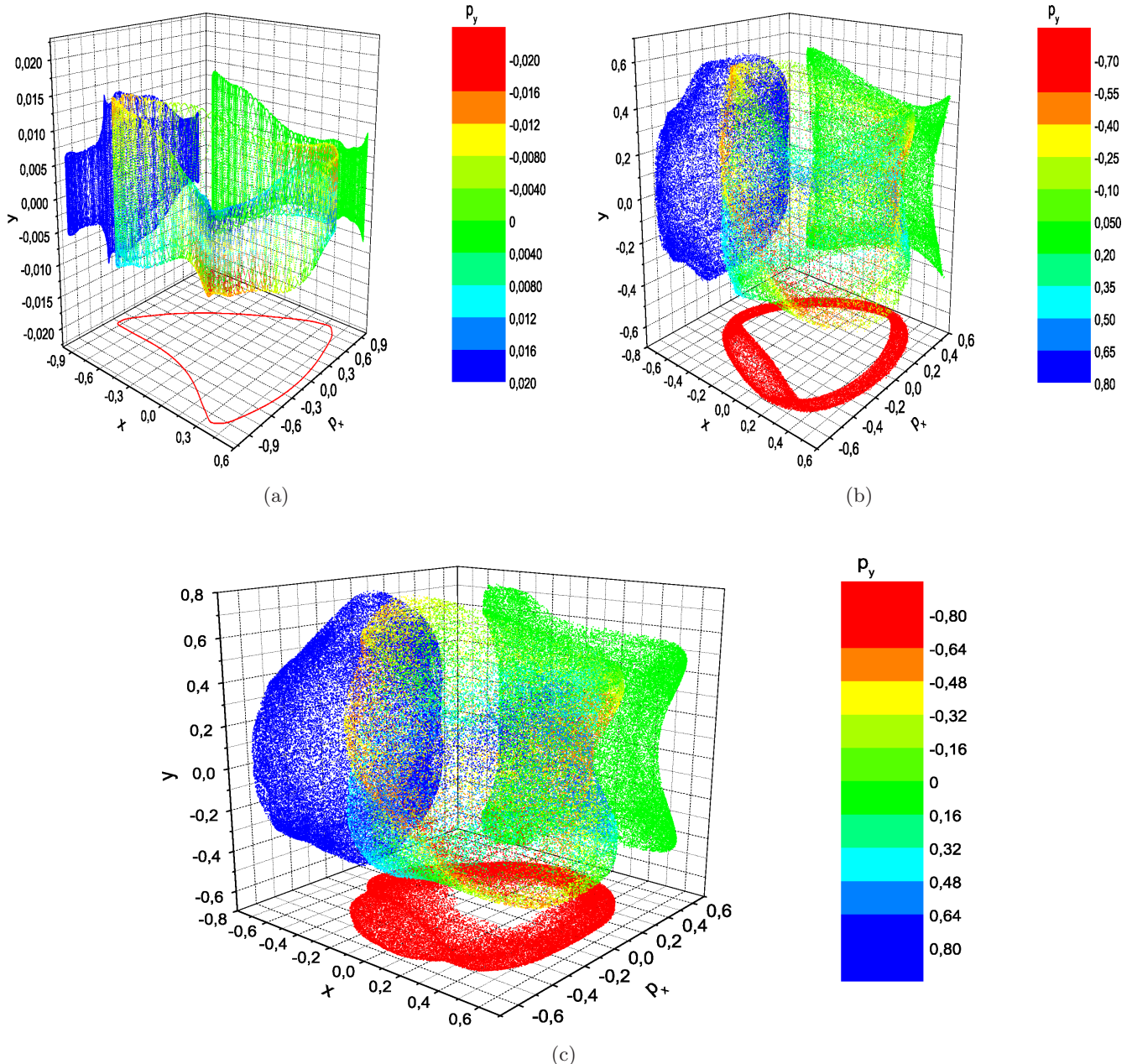


Fig. 3. (a) 3D and 2D projections of object 1 of the 4D Hénon map produced by EEDS, with tunes $\nu_x = 0.61903$ and $\nu_y = 0.4152$. (b) Alike for object 2. (c) Similarly for object 3. In all cases, the vertical column corresponds to the scaling of the fourth coordinate p_y of the 4D Hénon map.

0.94, for object 2 it is nearly 2.03, while the correlation dimension for object 3 is approximately 2.74.

Let us now discuss these results in more detail: Object 1 does not escape to infinity for 10^8 iterations of the map, and is located at a bigger distance from the origin than objects 2 and 3. However, since its dimension is close to 1 it corresponds to a single orbit and is hence of little importance in our search for a “final frontier” of bounded motion.

Object 2 does not escape to infinity for nearly 1.9×10^6 iterations of the map. Its correlation dimension is almost equal to 2, which implies that it must be close to an invariant torus. Indeed, we tried different orbits in its neighborhood and found that perturbing its p_x coordinate by -7.5×10^{-2} leads to a new “object” which has correlation dimension 2.001, average distance from the origin 0.66 with maximum distance 0.83 and minimum 0.50. It is invariant up to 10^8 iterations

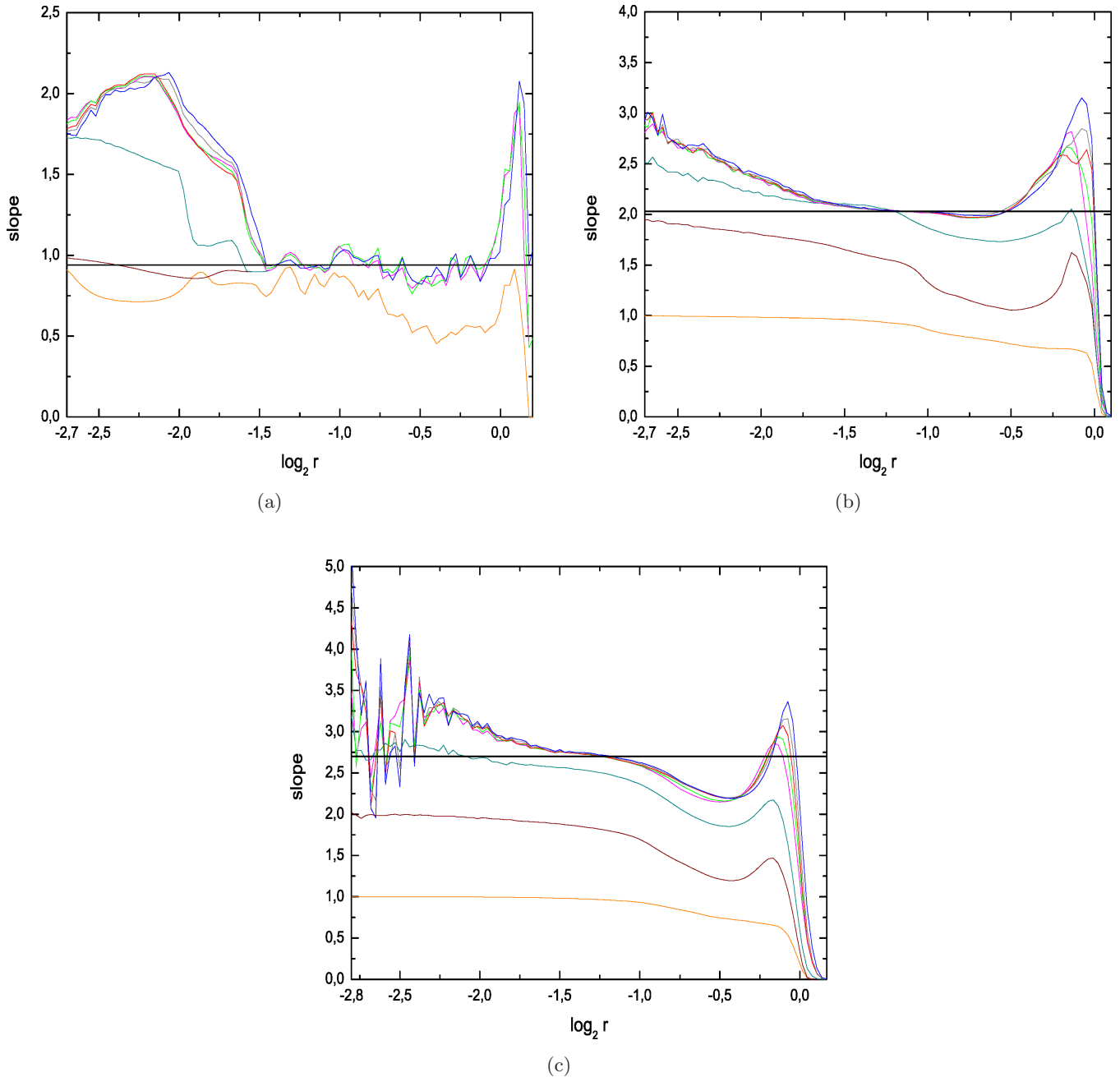


Fig. 4. (a) Estimation of the correlation dimension plotting the slope = $\log_2 C_2^d(r) / \log_2 r$ versus $\log_2 r$ for object 1 of the 4D Hénon map produced by EEDS. The horizontal black line is the slope ≈ 0.94 . (b) Similarly for object 2 of the 4D Hénon map. The horizontal black line is the slope ≈ 2.03 . (c) Similarly for object 3 the horizontal black line is the slope ≈ 2.74 . In all cases, the tunes are $v_x = 0.61903$ and $v_y = 0.4152$.

of the map and thus represents a much better approximation of the desired “object”. In Fig. 6, its 3D projection and the corresponding 2D dimensions are shown, while in Figs. 7(a) and 7(b) we present plots for the estimation of its correlation dimension.

Object 3 escapes to infinity after 621776 iterations of the map. As it is evident from Fig. 3(c),

it has the structure of a dense fractal set and surrounds object 2. Its shape is similar to that of a torus, but is, in fact, so close to a chaotic orbit, that it finally escapes to infinity.

From the above analysis we can draw the following conclusions: The application of EEDS for the 4D map leads in most cases to the discovery of objects which are close to invariant tori. Also very

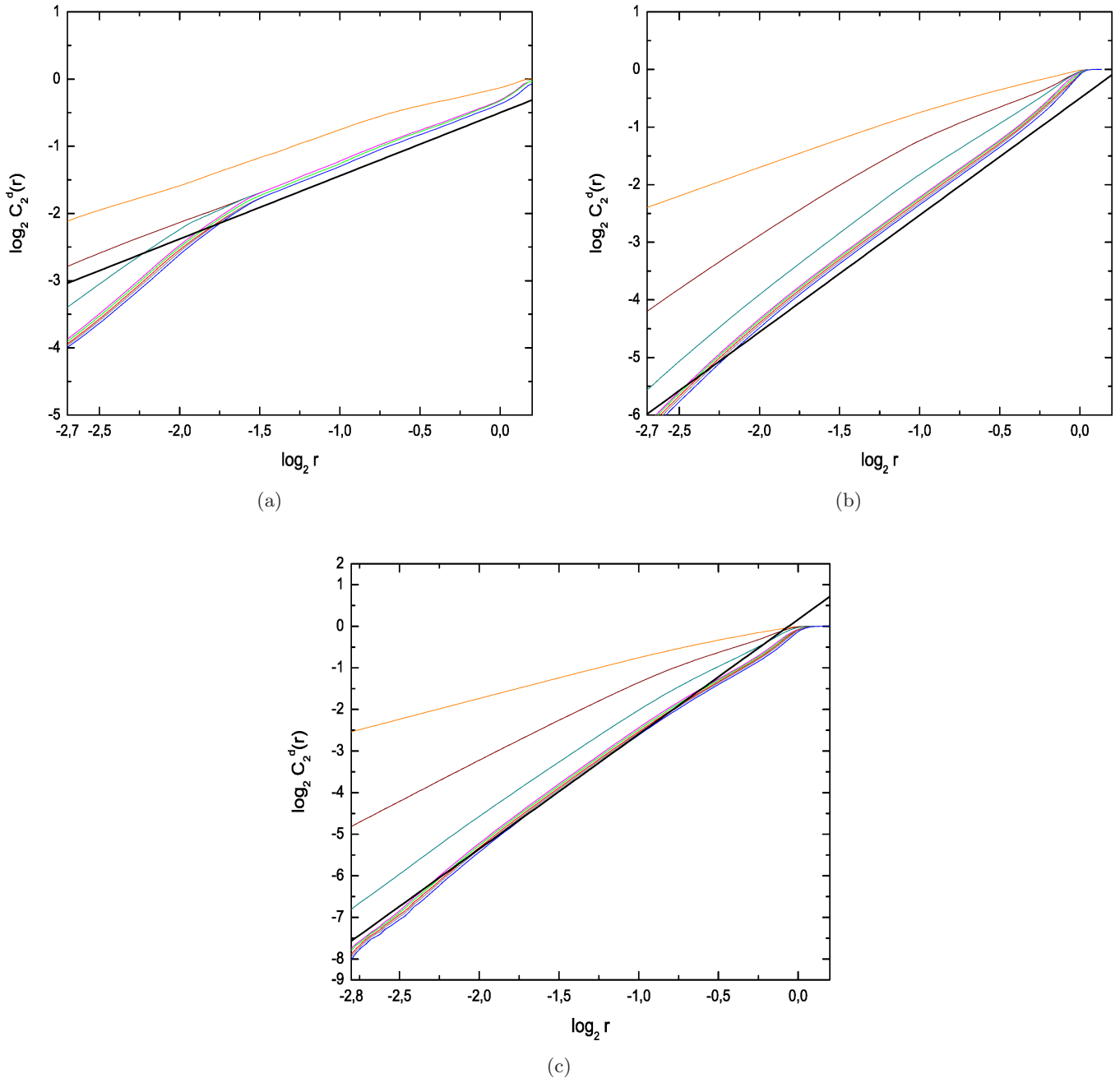


Fig. 5. (a) Estimation of the correlation dimension plotting $\log_2 C_2^d(r)$ versus $\log_2 r$ for object 1 of the 4D Hénon map produced by EEDS for the tunes $\nu_x = 0.61903$ and $\nu_y = 0.4152$. The black line corresponds to the linear fitting with slope ≈ 0.94 . (b) Similarly for object 2. The black line corresponds to the linear fitting with slope ≈ 2.03 . (c) Similarly, for object 3. The black line corresponds to the linear fitting with slope ≈ 2.74 .

close to these tori, EEDS can locate objects which are dense fractal sets (remaining bounded up to 6×10^5 iterations) and whose correlation dimension is approximately very close to 3. These results agree very well with a previous study [Vrahatis *et al.*, 1997], where invariant tori were found whose small perturbations led to fractal sets with correlation dimension nearly 3.

4.3. Application of EFO to the estimation of dynamic aperture

4.3.1. The case of the 2D Hénon map

The number of individuals of the DE algorithm used in the EFO method are set to 8 and the frequency ν_x of the 2D map lies in the interval $[0.01, 0.45]$. All frequencies produced during the execution of

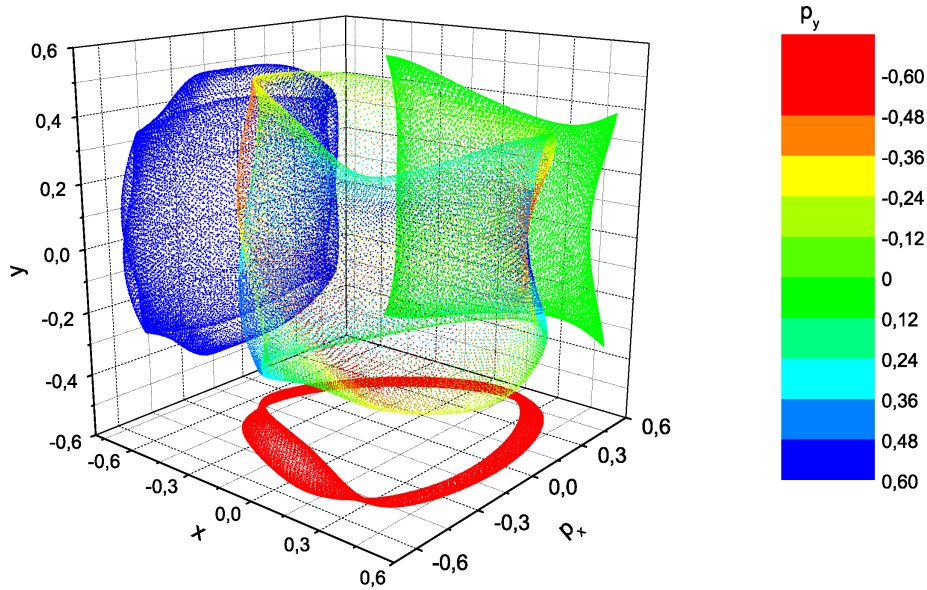


Fig. 6. 3D and 2D projections of the perturbation of object 2 of the 4D Hénon map produced by EEDS for tunes $v_x = 0.61903$ and $v_y = 0.4152$. The vertical column corresponds to the scaling of the fourth coordinate p_y of the 4D Hénon map.

EFO are restricted to lie in this interval, since the dynamic aperture for the 2D Hénon map near the tune $v_x = 0.5$ goes to infinity. Thus we start using EEDS with a population of ten individuals for the DE algorithm and setting its factors, F , CR equal

to 0.5. The chaotic threshold for the SALI method was set at the value 10^{-8} , while for the bisection method the threshold was set to 10^{-6} . The goal of the DE is to find the minimum distance between the elliptic point and the computed domain of stability

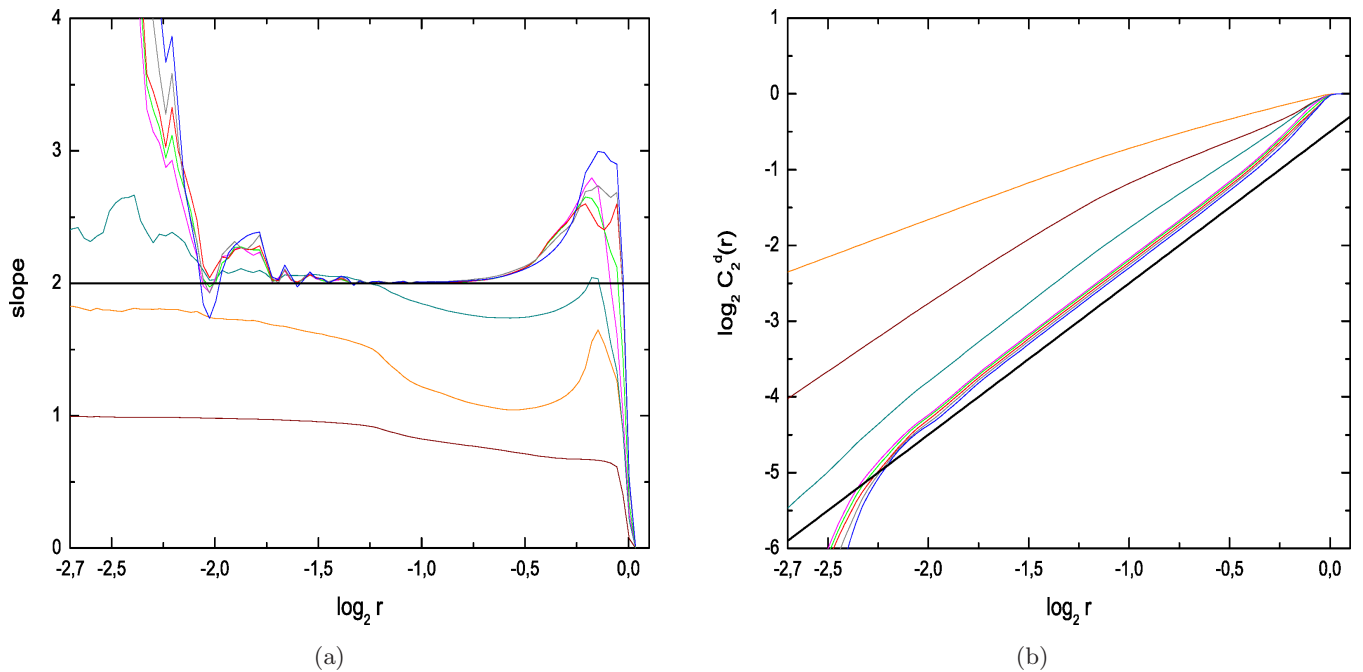


Fig. 7. (a) Estimation of the correlation dimension using the plot slope = $\log_2 C_2^d(r) / \log_2 r$ versus $\log_2 r$ for object 2 of the 4D Hénon map produced by EEDS for tunes $v_x = 0.61903$ and $v_y = 0.4152$. The horizontal black line is the slope ≈ 2.0 . (b) Complementary estimation of the correlation dimension making direct use of the plot of $\log_2 C_2^d(r)$ versus $\log_2 r$. The black line corresponds to the linear fitting with slope ≈ 2.03 .

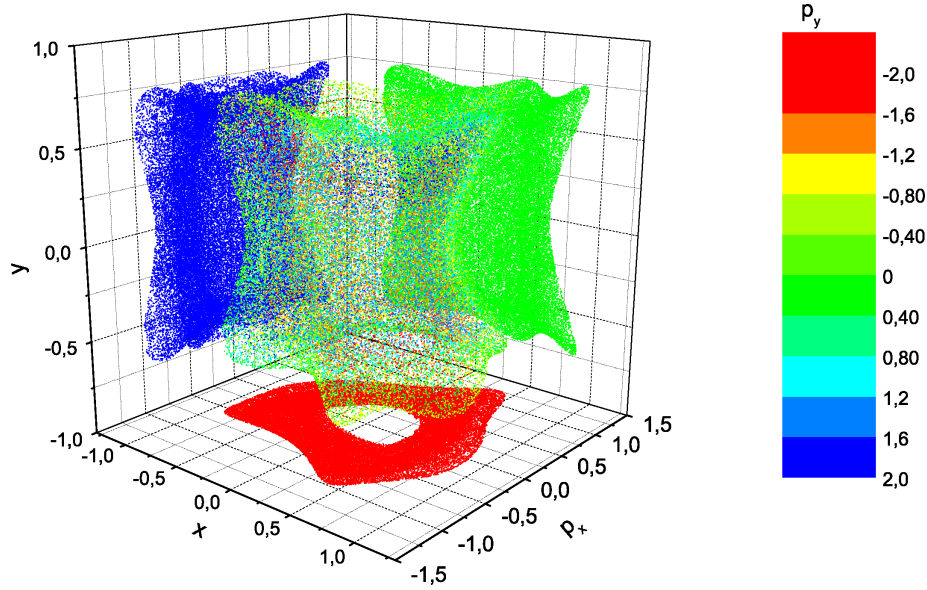


Fig. 8. 3D and the corresponding 2D projections of the “object” produced by EFO in the case of the 4D Hénon map for tunes $v_x = 0.596857$, $v_y = 0.500648$. The vertical column corresponds to the scaling of the fourth coordinate p_y of the 4D Hénon map.

of the 2D map. The objective function used here has the biggest weight in the second factor (see Sec. 3.2). The *best* frequency resulting from the prescribed methodology was found to be $v_x = 0.45$ [see Figs. 2(a) and 2(b)], a result also confirmed by directly iterating the 2D map.

4.3.2. The case of the 4D Hénon map

In the experiments concerning the 4D Hénon map, the number of individuals of DE used in EFO is set to 8 and the mutation and crossover factors are 0.5. The tunes are chosen to lie in the intervals $v_x = [0.1, 0.8]$ and $v_y = [0.2, 0.6]$ respectively. Our aim is to examine how the EFO method performs in this case. To this end, we choose randomly v_x, v_y tunes very close to the values used in Sec. 4.2. In realistic accelerator applications, of course one has to take into account the technological constraints required to apply EFO. The settings for EEDS require a population of ten individuals for the DE algorithm. The chaotic threshold for the SALI method is fixed at 10^{-8} , while for the bisection method it is 10^{-6} . The number of iterations of the map used in the computation of the SALI method was 5000 and when SALI was used combined with the bisection method it was 1000. Again, the goal of the DE used in EEDS is to find the minimum distance between the elliptic point and the computed “object”, following the approach described in the previous sections.

In several EEDS experiments of the 4D map, we noticed that, for the same frequencies, different objects were produced with different correlation dimensions. For this reason, for every individual frequency we applied our approach as many times as needed to obtain an “object” with the maximum possible correlation dimension for the necessary computations of the objective function. Ten points were selected randomly from this “object” to provide the perturbations. Each point was perturbed from 10^{-6} to 10^{-1} with six steps, each multiplied by 10. The maximum number of map iterations for the perturbed points was set to 10^8 . The first and second factors of the objective function are normalized in the interval $[0, 1]$. In the objective function, the first factor occurs with the biggest weight, while the other two have smaller weights.

Thus, we discovered that the output frequencies of the EFO method are $v_x = 0.596857$ and $v_y = 0.500648$, while the coordinates of the last point are

$$\begin{aligned} x &= -0.738012, & p_x &= -0.081621, \\ y &= 0.006851, & p_y &= 0.036232, \end{aligned}$$

yielding an orbit that remains stable up to 10^8 iterations. The mean distances of this orbit from the central point is 1.32 with standard deviation 0.29 and the dimension found for this “object” is close to 2.91.

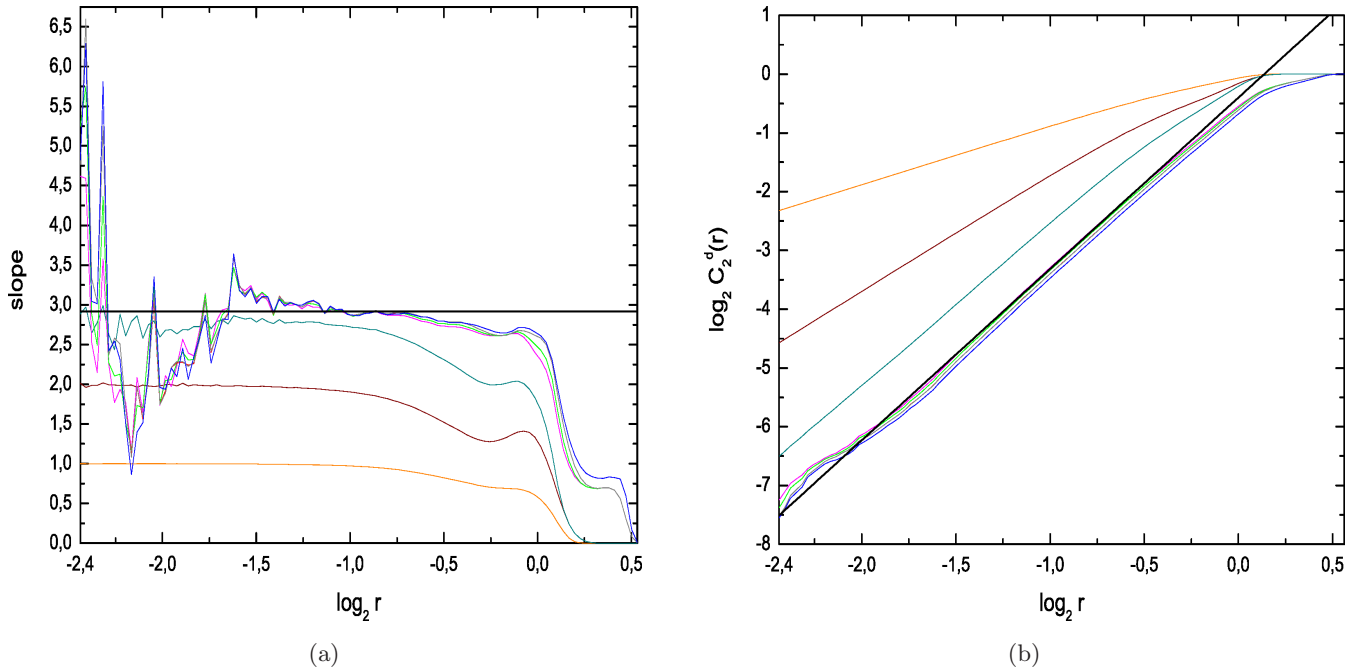


Fig. 9. (a) Estimation of the correlation dimension using the plot $\text{slope} = \log_2 C_2^d(r) / \log_2 r$ versus $\log_2 r$ for the “object” produced by EFO in the case of the 4D Hénon map for the tunes $v_x = 0.596857$, $v_y = 0.500648$. The horizontal black line indicates a “plateau” of the original plot, which constitutes an estimation of the correlation dimension at the slope ≈ 2.91 . (b) Estimation of the correlation dimension using the plot $\log_2 C_2^d(r)$ versus $\log_2 r$ for the “object” produced by EFO in the case of the 4D Hénon map for tunes $v_x = 0.596857$, $v_y = 0.500648$. The slope ≈ 2.91 of the line is an estimation of the correlation dimension.

It is worth mentioning that when we truncate the output pair of tunes to the values $v_x = 0.597$ and $v_y = 0.501$, the resulting “object” remains again stable up to 10^8 iterations having also, practically, the same correlation dimension as the initial result. However, the mean distance now is 1.14 with standard deviation 0.23. These observations lead to the conclusion that the output frequencies of EFO are robust under significant perturbations and retain the properties of the initial output “object”. This is of crucial importance to the experimentalists who can only adjust the frequencies of the machine up to few significant decimal digits, thus achieving the long term stability of the “object” produced by EFO.

In Fig. 8, a 3D projection of this “object” is shown along with the corresponding 2D projections for $v_x = 0.596857$ and $v_y = 0.500648$. The estimation of the correlation dimension is calculated with the help of the plots appearing in Figs. 9(a) and 9(b). In the first of them, the correlation dimension is estimated from the “plateau” that appears in the horizontal line, having a value around 2.91. In the second figure, the slope of the lines for $m \geq 4$ is the estimation of the correlation dimension.

The application of the linear fitting method also gives for this slope a value close to 2.91.

5. Conclusions

In this paper, we proposed first the method of the Evolutionary Estimation of the Domain of Stability (EEDS) to numerically approximate the dynamic aperture, or stability domain which contains the maximum possible “volume” of bounded orbits in symplectic mapping models of accelerator dynamics. Its application to the FODO cell maps was presented and was shown to yield very satisfactory results. In the 2D case, where we could check our predictions more easily, the dynamic aperture approximated by the proposed method was found to be quite close to the “last invariant curve” found by straightforward inspection methods. Furthermore, in the 4D case we found objects very close to a two-dimensional “last” invariant torus of the map and also objects nearby with fractal dimension close to 3, “surrounding” the last invariant torus.

Finally, global stability results were obtained by the second method proposed in this paper, called the Evolutionary Frequency Optimization (EFO),

which searches over large intervals of values of the frequency(ies) of the map, using EEDS to estimate the corresponding dynamical aperture. The best such “object” was achieved for $v_x = 0.596857$, $v_y = 0.500648$, having correlation dimension close to 2.9 and yielding bounded orbits up to 10^8 iterations of the map.

It is important to note that the proposed methods are not restricted to symplectic maps. They can also be applied to volume preserving maps which are not symplectic as well as to continuous dynamical systems (flows) and can also be generalized to treat conservative dynamical systems of any dimension. Furthermore, the EEDS method can be used, with minor modifications, to approximate the stability domain of any interior region of phase space surrounded by chaos.

In a future publication we intend to apply the proposed methods to accelerator maps with dimension greater than 4, taking into account also the motion of the particles in the longitudinal direction. Finally, we also plan to study maps which model more realistic beams, where periodic modulations of the tunes, due e.g. to the so-called space charge effects [Bountis & Skokos, 2006b], need to be taken into consideration.

Acknowledgments

This work was partially supported by the European Social Fund (ESF), Operational Program for Educational and Vocational Training II (EPEAEK II) and particularly the Program PYTHAGORAS II, supporting in part the research of C. G. Antonopoulos and T. C. Bountis. Finally, we would like to thank Assistant Professor D. Kugiumtzis for his invaluable help on the estimation of the correlation dimension.

References

- Antonopoulos, Ch. & Bountis, T. C. [2006a] “Stability of simple periodic orbits and chaos in a Fermi–Pasta–Ulam lattice,” *Phys. Rev. E* **73**, 056206, 1–8.
- Antonopoulos, Ch., Bountis, T. C. & Skokos, Ch. [2006b] “Chaotic dynamics of N -degree of freedom Hamiltonian systems,” *Int. J. Bifurcation and Chaos* **16**, 1–18.
- Bazzani, A., Todesco, E., Turchetti, G. & Servizi, G. [1994] “A normal form approach to the theory of nonlinear betatronic motion,” *CERN, Yellow Reports*, 94–02.
- Bountis, T. & Skokos, Ch. [2006a] “Application of the SALI chaos detection method to accelerator mappings,” *Nuclear Instrum. Meth. Phys. Res. Section A* **561**, 173–179.
- Bountis, T. & Skokos, Ch. [2006b] “Space charges can significantly affect the dynamics of accelerator maps,” *Phys. Lett. A* **358**, 126–133.
- Chirikov, B. V. [1979] “A universal instability of many-dimensional oscillator systems,” *Phys. Rep.* **52**, 263–379.
- Corne, D., Dorigo, M. & Glover, F. [1999] *New Ideas in Optimization* (McGraw–Hill, London).
- De Assis, L. P. G., Helayel Neto, J. A., Haas, F. & Nogueira, A. L. M. A. [2005] “On the integrability and chaos of an $n = 2$ Maxwell–Chern–Simons–Higgs mechanical model,” hep-th/0505159, preprint.
- Engelbrecht, A. P. [2002] *Computational Intelligence: An Introduction* (John Wiley).
- Grassberger, P. & Procaccia, I. [1983a] “Characterization of strange attractors,” *Phys. Rev. Lett.* **50**, 346–349.
- Grassberger, P. & Procaccia, I. [1983b] “Measuring the strangeness of strange attractors,” *Physica D* **9**, 180–208.
- Hegger, R., Kantz, H. & Schreiber, T. [1999] “Practical implementation of nonlinear time series methods: The TISEAN package,” *Chaos* **9**, 413–435.
- MacKay, R. S. & Meiss, J. D. (eds.) [1987] *Hamiltonian Dynamical Systems* (Adam Hilger, Bristol).
- Manos, T. & Athanassoula, E. [2005a] “Chaos and the dynamical evolution of barred galaxies,” astro-ph/0510823, preprint.
- Manos, T. & Athanassoula, E. [2005b] “Detecting chaotic and ordered motion in barred galaxies,” astro-ph/0510824, preprint.
- Meiss, J. D. [1992] “Symplectic maps, variational principles and transport,” *Rev. Mod. Phys.* **63**, 795–847.
- Panagopoulos, P., Bountis, T. & Skokos, Ch. [2004] “Existence and stability of localized oscillations in 1-dimensional lattices with soft spring and hard spring potentials,” *J. Vibr. Acoust.* **126**, 520–527.
- Plagianakos, V. P. & Vrahatis, M. N. [2002] “Parallel evolutionary training algorithms for “hardware-friendly” neural networks,” *Natural Comput.* **1**, 307–322.
- Scandale, W. & Turchetti, G. (eds.) [1991] *Nonlinear Problems in Future Particle Accelerators* (World Scientific, Singapore).
- Skokos, Ch. [2001] “Alignment indices: A new, simple method for determining the ordered or chaotic nature of orbits,” *J. Phys. A* **34**, 10029–10043.
- Skokos, Ch., Antonopoulos, Ch., Bountis, T. C. & Vrahatis M. N. [2003a] “How does the Smaller ALignment Index (SALI) distinguish order from chaos?” *Progr. Theoret. Phys. Suppl.* **150**, 439–443.

- Skokos, Ch., Antonopoulos, Ch., Bountis, T. C. & Vrahatis, M. N. [2003b] “Smaller ALignment Index (SALI): Determining the ordered or chaotic nature of orbits in conservative dynamical systems,” in *Proc. Conf. Libration Point Orbits and Applications*, eds. Gomez, G., Lo, M. W. & Masdemont, J. J., pp. 653–664.
- Skokos, Ch., Antonopoulos, Ch., Bountis, T. C. & Vrahatis, M. N. [2004] “Detecting order and chaos in Hamiltonian systems by the SALI method,” *J. Phys. A* **37**, 6269–6284.
- Storn, R. & Price, K. [1997] “Differential evolution — a simple and efficient heuristic for global optimization over continuous spaces,” *J. Global Optim.* **11**, 341–359.
- Széll, A. [2003] *Investigation of the Caledonian Symmetrical Four-Body Problem*, PhD thesis, Glasgow Caledonian University.
- Széll, A., Érdi, B., Sándor, Zs. & Steves, B. [2004] “Chaotic and stable behavior in the caledonian symmetric four-body problem,” *Monthly Not. Roy. Astron. Soc.* **347**, 380–388.
- Todesco, E. & Giovannozzi, M. [1996] “Dynamic apertures estimates and phase-space distortions in nonlinear betatron motion,” *Phys. Rev. E* **53**, 4067–4076.
- Vrahatis, M. N. [1995] “An efficient method for locating and computing periodic orbits of nonlinear mappings,” *J. Comput. Phys.* **119**, 105–119.
- Vrahatis, M. N., Isliker, H. & Bountis, T. C. [1997] “Structure and breakdown of invariant tori in 4D mapping model of accelerator dynamics,” *Int. J. Bifurcation and Chaos* **7**, 2707–2722.